Journal of Magnetism and Magnetic Materials, Volume 473, pp. 148-154, 2019.
DOI: 10.1016/j.jmmm.2018.10.070

Enhanced specific loss power from Resovist® achieved by aligning magnetic easy axes of nanoparticles for hyperthermia

Guannan Shi[a*], Ryoji Takeda[a], Suko Bagus Trisnanto[a], Tsutomu Yamada[a], Satoshi Ota[b], Yasushi Takemura[a]

[a]Department of Electrical and Computer Engineering, Yokohama National University, Yokohama 240-8501, Japan
[b]Department of Electrical and Electronic Engineering, Shizuoka University, Hamamatsu 432-8561, Japan
*guannan-shi-hr@ynu.jp

In this study, we precisely calculated the specific loss powers (SLPs) of magnetic nanoparticles (MNPs) based on dynamic hysteresis measurements. The advantage of this evaluation method is that the intensity and frequency of the applied magnetic field can be varied over a wide range for samples of various condition. The results show that the coercive field and SLP of Resovist® increase by orienting the magnetic easy axes of the nanoparticles. The magnetic field was applied either parallel or perpendicular to the nanoparticle orientation. The area enclosed by the dynamic hysteresis curve was larger when the AC field was applied parallel to the nanoparticle orientation, indicating a greater increase in the hyperthermia temperature. This characteristic originated from the magnetic anisotropy energy of the nanoparticles and is in good agreement with our simulational results. The SLP of a solid sample with an aligned easy axis measured under an AC field of 4 kA/m, which was applied parallel to the axis, was more than two times that of a liquid sample. We also evaluated the SLPs of superparamagnetic 4-nm-diameter γ-Fe_2O_3 and ferromagnetic 20–30-nm-diameter Fe_3O_4 MNPs and compared them to that of Resovist®.

Keywords: magnetic nanoparticles; hyperthermia; specific loss powers; coercive field; easy axis; anisotropy energy

Journal of Magnetism and Magnetic Materials, Volume 473, pp. 148-154, 2019.
DOI: 10.1016/j.jmmm.2018.10.070

1 Introduction

Magnetic nanoparticles (MNPs) are widely applied to biomedical applications such as magnetic fluid hyperthermia (MFH)[1], magnetic particle imaging (MPI)[2], and drug delivery systems (DDSs)[3]. They are also attracting much attention as theranostics agents, which means that treatment and diagnosis can be performed in a single system[4,5]. A commercially available MNP, called Resovist® (FUJIFILM RI Pharma), is a contrast agent for magnetic resonance imaging (MRI). It is also widely used for research on MFH[6] and MPI[7]. The specific loss power (SLP), which is also called specific absorption rate (SAR), indicates the amount of heat generated by the MNPs for MFH. In the conventional study, it is revealed that the heating performance is determined by the size, anisotropy, and saturation magnetization as the parameter of MNPs, the dosage of MNPs in tumor, and the condition of the applied field such as the field intensity and frequency[8]. The estimation of the SLP considering the volume of the target tumor is also important for the clinical efficacy[9]. To achieve a high SLP, the magnetic properties of Resovist® need to be investigated, and optimal conditions related to the applied field and the parameters of Resovist® should be determined. In this study, we fabricated samples of Resovist® with oriented easy axes[10,11] and measured their magnetic properties. The orientation of the easy axes should be considered for MFH applications wherein an AC magnetic field is employed for diagnosis. Moreover, it is important to clarify the magnetic properties of MNPs under an AC field in terms of the degree of anisotropy. In this study, we obtained the magnetization curves for Resovist® with oriented easy axes under an AC magnetic field with a frequency in the range of 1–100 kHz, considering their relaxation properties.

The energy of MNPs under an external magnetic field can be divided into two parts: anisotropy energy and energy associated with the external magnetic field[12]. When an AC magnetic field is applied to MNPs, a magnetic relaxation occurs because of the delay in the magnetization of the magnetic field. The Néel relaxation time τ_N and the Brownian relaxation time τ_B can be derived from the rotation of the magnetic moment and the rotation of the magnetic particles, respectively. The Néel relaxation time can be expressed as follows.

$$\tau_N = \tau_0 \exp\left(\frac{K_u V_M}{k_B T}\right) \quad (1)$$

where τ_0, T, and k_B denote the attempt time, temperature, and Boltzmann constant, respectively[13,14]. If Brownian relaxation and Néel relaxation occur simultaneously, the effective relaxation time τ_{eff} for the MNPs can be expressed as follows.

$$\tau_{eff} = \left(\frac{1}{\tau_B} + \frac{1}{\tau_N}\right)^{-1} \quad (2)$$

However, according to Equation (2), Néel relaxation largely decides the effective relaxation time for particles with a small core size[15], though Brownian relaxation has been experimentally observed[16]. The relaxation time of an effective magnetic relaxation cannot be simply obtained using Equation (2). In contrast to the conventional theory of the effective relaxation, the Brownian relaxation superimposed to the Néel relaxation was observed[17]. The dynamics of the easy axis derived from the Brownian relaxation was numerically and empirically observed[18,19]. Moreover, the Brownian relaxation occurred after the

Néel relaxation was clearly detected by applying a pulse field in the transitional response of the magnetization and easy axis[20)].

The magnetic relaxations generate thermal energy. The method of calculating the SLP by the calorimetric measurement has been reported[21)]. The SLP is principally derived by the time change rate of temperature when magnetic field is applied[22)]. In this study, we show that the SLP can be accurately calculated based on dynamic hysteresis measurements. It has also been reported that the calculated SLP values depend on the method of analyzing the temperature rise curve and on the shape of the sample even when the same particle and excitation condition are used[23)]. However, the method of estimating the SLP from the AC hysteresis curve can eliminate the difficulties associated with measuring the temperature[24,25)]. This evaluation method is expected to accurately determine the SLP values. Moreover, the SLP of MNPs inside living cells was estimated from the measurement of the AC magnetization curves[26,27)]. Further, we discussed ways of increasing the SLP and the hyperthermia temperature. The obtained results are essentially different from those of hyperthermia experiments conducted under an applied AC magnetic field superimposed by a DC one, in which case the SLP reduces.

2 Materials and methods

2.1 Materials

Resovist® (commercially distributed by FUJIFILM RI Pharma) is γ-Fe_2O_3 particles, which have a core size in the range of 5–10 nm[18)], and a hydrodynamic size of 75 nm measured by dynamic light scattering for the coated with carboxydextran in water. It is not only used as a contrast agent in MRI but also as a tracer of MPI[7)] and a heating source for hyperthermia[6)]. Although Resovist® exhibits superparamagnetism owing to its small core particle diameter, it has been reported that multicore particles effectively behave as a single particle[28)] with a wide particle size distribution[29)].

Figure 1 shows the preparation processes of the liquid and solid samples. Two types of solid samples were prepared for Resovist®. The solution of 15 μl of undiluted Resovist® with concentration of 28 mg-Fe/ml was dispersed into purified water or epoxy for preparing the liquid or solid sample of 0.2 ml, respectively. For the solid sample, the MNPs were mixed with the epoxy bond (CEMEDINE Co.). The epoxy consisted of epoxy resin (viscosity of 100.0 Pa·s at 23 ºC, density of 1.14 mg/mm^3) and polyamide (viscosity of 50.0 Pa·s at 23 ºC, density of 0.99 mg/mm^3) at a volume ratio of 1:1. It turned to a solid state for 6 h after agitation for 5 min. The first sample contains MNPs held together using an epoxy bond in the absence of magnetic field, whereas the other sample contains MNPs under a DC magnetic field applied using an electromagnet for 8 h. Accordingly, the easy axes of the MNPs in the first sample are randomly oriented, whereas the easy axes of the MNPs in the second sample are aligned in a particular direction. The first sample is called as the random sample. For the second sample with an aligned easy axis, the DC and AC measurements were taken by applying a magnetic field parallel and perpendicular to the easy axis; the samples thus obtained are called the easy axis sample and the hard axis sample, respectively. Figure 1 (a–d) shows the samples for experiment. The intensity of the DC field during the preparation of the samples with aligned easy axes was 575 kA/m[11)].

Journal of Magnetism and Magnetic Materials, Volume 473, pp. 148-154, 2019.
DOI: 10.1016/j.jmmm.2018.10.070

Liquid, random and oriented solid samples were also prepared, similar to the Resovist® samples, using superparamagnetic 4-nm-diameter γ-Fe_2O_3 and ferromagnetic 20–30-nm-diameter Fe_3O_4 MNPs[11)] to compare their properties with those of Resovist® of various sizes of multi-core particles. The water-dispersed γ-Fe_2O_3 nanoparticles with core diameters of 4 nm supplied from Meito Sanyo Co. Ltd. were used. They were coated with carboxymethyl-diethylaminoethyl dextran. Furthermore, the Fe_3O_4 nanoparticles with diameters of 20–30 nm purchased from Nanostructured and Amorphous Materials Inc. were used. They were coated with polyethylenimine. The primary concentrations of γ-Fe_2O_3 and Fe_3O_4 nanoparticles dispersed in purified water were 28 mg-Fe/mL and 3 mg-Fe/mL, respectively. The concentrations of the MNPs in all the samples used in this study were adjusted to 2 mg-Fe/ml.

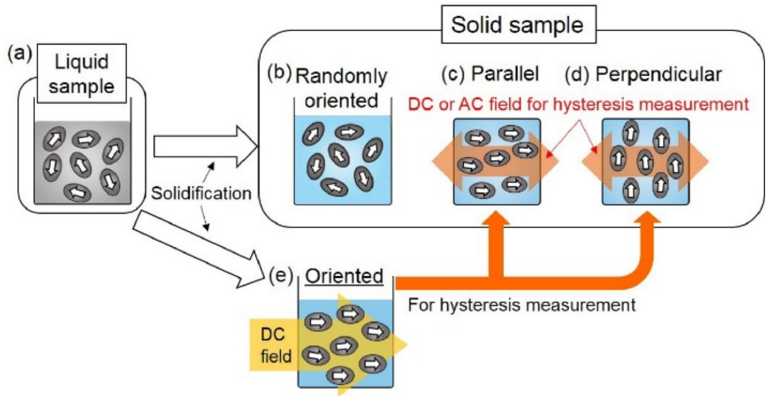

Fig. 1 Preparation process of oriented samples: (a) Liquid sample, (b) Randomly oriented sample, (c) Sample for experiment by applying a magnetic field parallel to easy axis, (d) Sample for experiment by applying a magnetic field perpendicular easy axis. And (e) Sample oriented by DC field.

2.2 Magnetization measurements

The DC magnetization curves were obtained using a vibrating sample magnetometer (VSM, TOEI KOGYO, VSM-5), and the AC magnetization curves were obtained at a frequency in the range of 1–100 kHz under applied field amplitudes of 4 and 16 kA/m using homemade AC magnetization device equipped with a 210-turn water-cooled solenoid coil with a diameter of 16.0 mm for excitation. The measurements were taken at a temperature of 298 K. A magnetic field intensity of 16 kA/m was adopted as a typical value range of the magnetic field for hyperthermia. The magnetic properties were also investigated under applied field intensity of 4 kA/m, which is easily achieved for body-size excitation and excitation at higher frequency. The saturation magnetizations of the samples were estimated by fitting the DC magnetization curve at a field intensity of 800 kA/m to plot the magnetization curve using the Langevin function. The same plastic tube was used as the sample holder for both liquid and solid samples. The diamagnetism of the sample holder, and water or epoxy bond was calibrated in the VSM measurement. The SLP was quantified by calculating the area of the AC hysteresis curve as the magnetic loss, including the magnetization relaxation loss. Just one AC hysteresis curve was used to calculate one value of the SLP. The intrinsic loss power (ILP) was derived by the equation: $ILP = SLP/H^2 \cdot f$, where H and f are the intensity and frequency of the applied AC excitation field, respectively[30)].

Journal of Magnetism and Magnetic Materials, Volume 473, pp. 148-154, 2019.
DOI: 10.1016/j.jmmm.2018.10.070

3 Results and discussion

3.1 DC magnetization curves

Figure 2 shows the DC magnetization curves of four samples at a field intensity of 800 kA/m. The magnetization is normalized using the saturation magnetization and is represented in the unit of M/M_s. When a magnetic field of 575 kA/m is employed in the fabrication of an oriented sample, the magnetization of the liquid sample is fully saturated. In addition, the magnetization of the randomly oriented sample is 0.96 M/M_s, indicating that the magnetization is sufficiently aligned in the direction of the exciting magnetic field at the time of orientation after solidification, though some particles that cannot be partially oriented are present. From the DC magnetization curve, the saturation magnetization of Resovist® was obtained as 94.4 $A{\cdot}m^2$/kg-Fe. Figure 3 shows the DC magnetization curves of the samples at field intensities of 4 and 16 kA/m. First, it is confirmed that the liquid sample does not exhibit a coercive field and remanent magnetization. As particles in the liquid sample rotate after DC or low frequency field has been applied, the magnetization curve of the liquid sample exhibits superparamagnetic-like property without any coercive field[31)].

On the other hand, the solid sample exhibits a small coercive field. This is because although Resovist® has a core particle diameter in the range of 5–10 nm, it forms several multicore particles exhibiting a wide particle diameter distribution ranging from 6.1 to 21.6 nm[29)]. Even in the case of 4 kA/m and 16 kA/m, the magnitude of the magnetization in the easy axis sample and hard axis sample were larger and smaller than that in the random oriented sample, respectively. In applying field of 4 kA/m and 16 kA/m, the magnetization in the easy axis sample was larger than that in the random oriented and hard axis samples. The magnetization in the hard axis sample was smaller than that in the random oriented sample. It is because the magnetization is bound to the easy axis due to the anisotropy energy and is easy to rotate toward the direction of the easy axis.

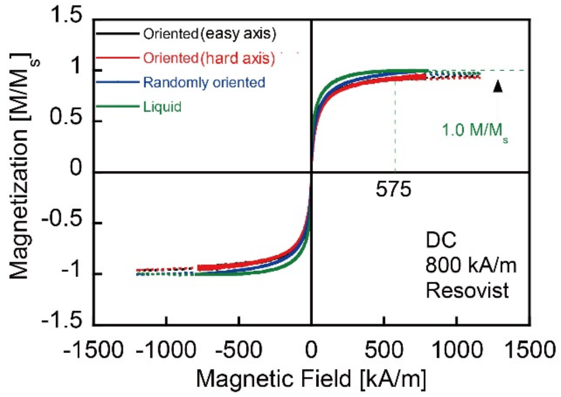

Fig. 2 DC magnetization curves of Resovist at a field intensity of 800 kA/m.

Journal of Magnetism and Magnetic Materials, Volume 473, pp. 148-154, 2019.
DOI: 10.1016/j.jmmm.2018.10.070

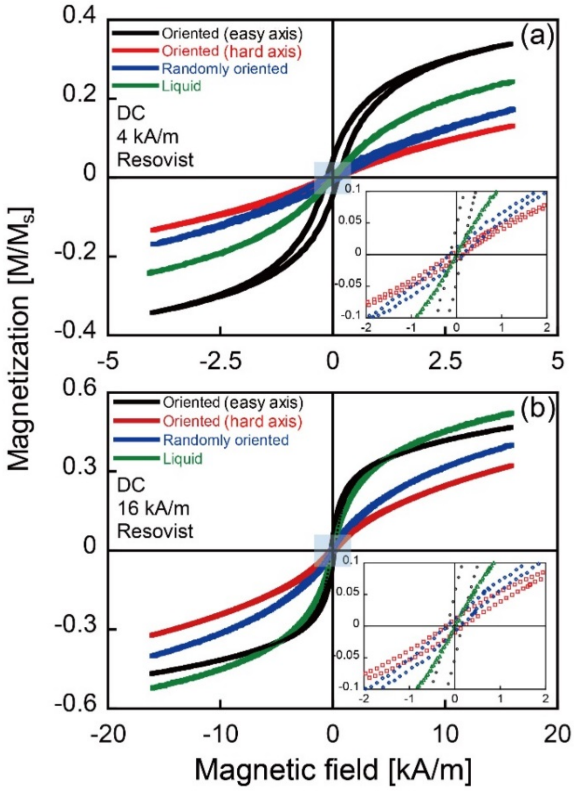

Fig. 3 DC magnetization curves at field intensities of (a) 4 kA/m and (b) 16 kA/m.

3.2 AC magnetization curves

Figure 4 shows the AC hysteresis curve at a field intensity of 4 kA/m. From the hysteresis curve, it is observed that the coercive field increases with the increase in the frequency in the easy axis sample, whereas the coercivity remains low in the hard axis sample even at a high frequency of 100 kHz. Figure 5(a) shows the frequency characteristics of the coercive fields of the easy axis sample, hard axis sample, random sample, and liquid sample at a magnetic field intensity of 4 kA/m. The coercive field tends to slightly increase with the increase in the frequency in the hard axis sample. On the contrary, the coercive field increases remarkably in the easy axis sample. The results of the DC hysteresis curve show that the magnetization in the easy axis sample is higher than that in the liquid sample in the applied field intensity of 4 kA/m.

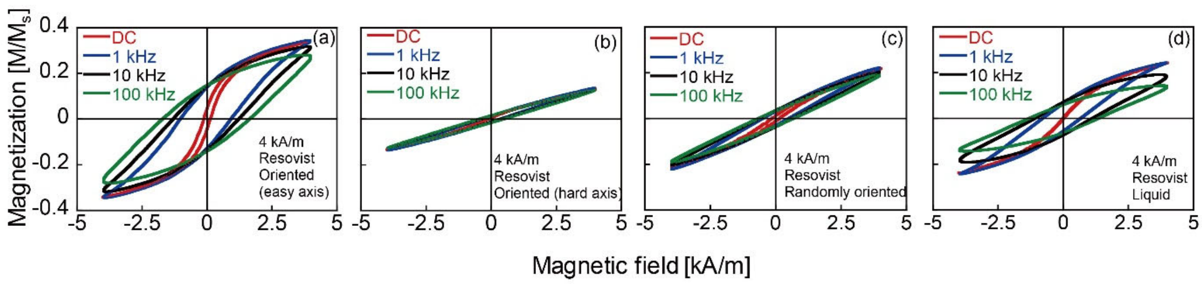

Fig. 4 DC and AC magnetization curves of Resovist® at a field intensity of 4 kA/m: (a) easy axis aligned

sample, (b) hard axis aligned sample, and (c) randomly oriented sample, and (d) liquid sample.

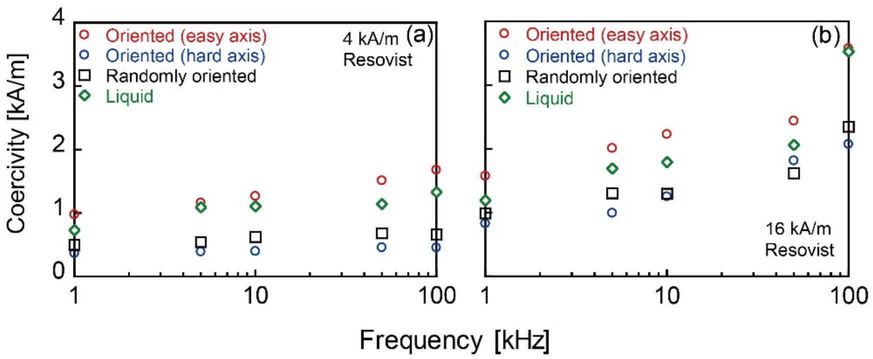

Fig. 5 Frequency characteristics of coercive field at magnetic field intensities of (a) 4 kA/m and (b) 16 kA/m.

Furthermore, the AC measurements were performed at a magnetic field intensity of 16 kA/m. Figure 6 shows the AC hysteresis curve at a field intensity of 16 kA/m. Figure 5(b) shows the frequency dependence of the coercive field. The increasing tendencies of the coercive field in the easy axis and hard axis samples are similar to those in the magnetic field intensity of 4 kA/m. We observed the change in the orientation of the magnetization by the numerically simulation with regard to the MNP in core diameter of 5±2 nm (mean±SD), when the field intensity was changed from –16 kA/m to 16 kA/m at the field frequency of 100 kHz[11)]. Our numerical simulation revealed that the magnetization is oriented to the opposite direction of the applied field without reversal in the easy axis sample because of the anisotropy toward the easy axis. On the other hand, the magnetization tends to align around the direction perpendicular to the excitation magnetic field in the hard axis sample. The degree of the orientation of the magnetization toward the direction of the applied field in the random sample is less than that in the easy axis sample. From the simulational result, it is considered that the magnetic moment induced by the AC magnetic field in the easy axis sample dominates the magnetization reversal. It is indicated that the coercive field increases because of the time delay between the magnetic field and magnetic moments with increase of the frequency, while exceeding the barrier of the anisotropy energy in the easy axis sample. In addition, the magnetization rotation with our reversal occurs in the hard axis sample, and the magnetization follows the excitation alternating magnetic field even at high frequencies. Hence, it is indicated that the Néel relaxation time in the hard axis sample was shorter than that in the random sample. It was also confirmed that the coercive fields in the easy axis and hard axis samples are larger and smaller than that in the random sample, respectively[10,11)].

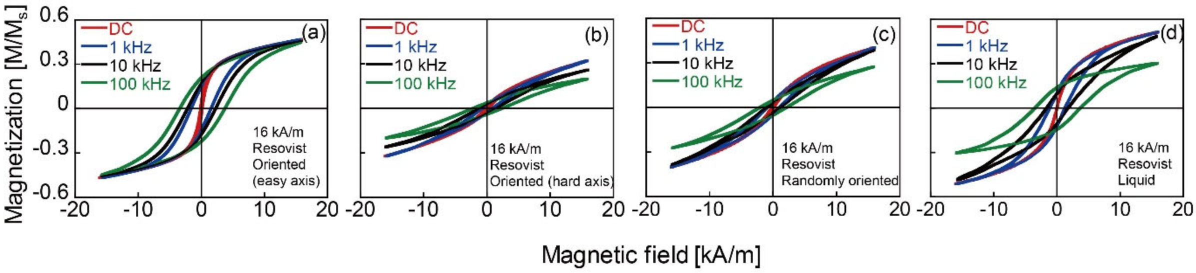

Fig. 6 DC and AC magnetization curves of Resovist® at a field intensity of 16 kA/m: (a) easy axis aligned sample, (b) hard axis aligned sample, and (c) randomly oriented sample, and (d) liquid sample.

Regarding the magnetization, at the AC magnetic field strength of 16 kA/m (Fig. 6(a–c)), the magnetization in the easy axis and hard axis samples were larger and smaller than that in the random sample, respectively. It is because the anisotropy due to the orientation of the easy axis appeared[32,33]. In addition, the magnetization of the liquid sample was larger than other samples. When the magnetic field intensity increases from 4 kA/m to 16 kA/m, the magnetic torque increases[34]. The magnetization tends to orient toward the direction of the applied field and is particularly bound to the easy axis in the high field intensity[26]. It is indicated that in the field intensity of 16 kA/m, the magnetization remains in the opposite direction to the applied field without reversal in the easy axis sample because of the anisotropy toward the easy axis. Especially, in the case of DC field and AC field in low frequency, it is indicated that residual components of the magnetization without reversal is low in the liquid sample compared to the case in the easy axis sample because the easy axis is oriented so as to follow the magnetization in liquid sample. Thus, the magnetization in the liquid sample is larger than that of the easy axis sample at 16 kA/m owing to the rotation of the easy axis.

We also evaluated magnetic properties of solid oriented samples of γ-Fe_2O_3 in the core diameter of 4 nm, γ-Fe_2O_3 (4 nm), and Fe_3O_4 in the core diameter of 20–30 nm, Fe_3O_4 (20–30 nm). Major curves of DC magnetization and minor curves of AC magnetization of these samples have been previously reported[11]. Other magnetization properties of DC and AC minor curves are shown in Supplementary section. As seen in those results, γ-Fe_2O_3 (4 nm) exhibited typical superparamagnetic properties, whereas Fe_3O_4 (20–30 nm) exhibited ferromagnetic properties with coercive field. As shown in Figs. 7 and 8, the coercivity of Resovist® used in this study is compared with those of the two oriented samples. Each particle has a high coercive field in the easy axis sample and a low coercive field in the hard axis sample at magnetic fields of 4 and 16 kA/m[10,11,32]. γ-Fe_2O_3 (4 nm) exhibits extremely low coercive field because of superparamagnetism, however, Resovist® exhibits a higher coercive field than γ-Fe_2O_3 (4 nm) in both the easy axis and hard axis samples. The influence of the long Néel relaxation time associated with large particles is evident because of the wide particle size distribution of Resovist®[29]. On the other hand, Fe_3O_4 (20–30 nm) exhibits a low coercive field without causing magnetization reversal at a magnetic field of 4 kA/m; however, it exhibits a high coercive field due to magnetization reversal at a magnetic

Journal of Magnetism and Magnetic Materials, Volume 473, pp. 148-154, 2019.
DOI: 10.1016/j.jmmm.2018.10.070

field of 16 kA/m. The part of the magnetization in Fe_3O_4 (20–30 nm) is not reversed when the intensity of the applied field is not enough high for the magnetization to overcome the anisotropy energy barrier. Because the potential energy in the applied field of 16 kA/m is reduced compared with that in 4 kA/m[12], the coercive field in 16 kA/m is higher than that in 4 kA/m.

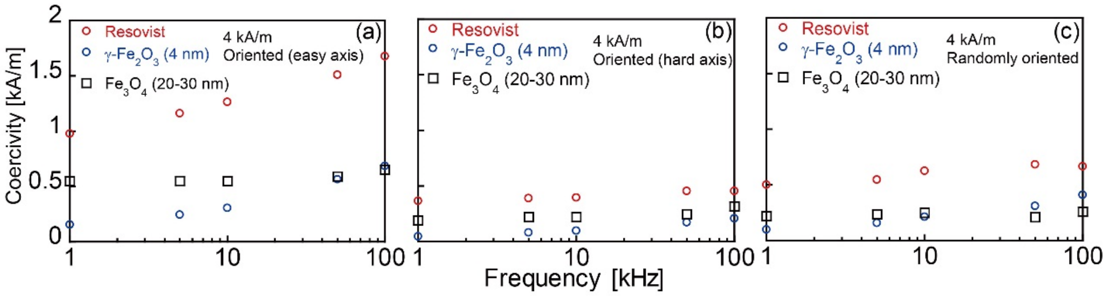

Fig. 7 Frequency characteristics of coercive fields of Resovist, γ-Fe_2O_3, and Fe_3O_4 for (a) easy axis aligned sample, (b) hard axis aligned sample, and (c) randomly oriented sample at a magnetic field of 4 kA/m.

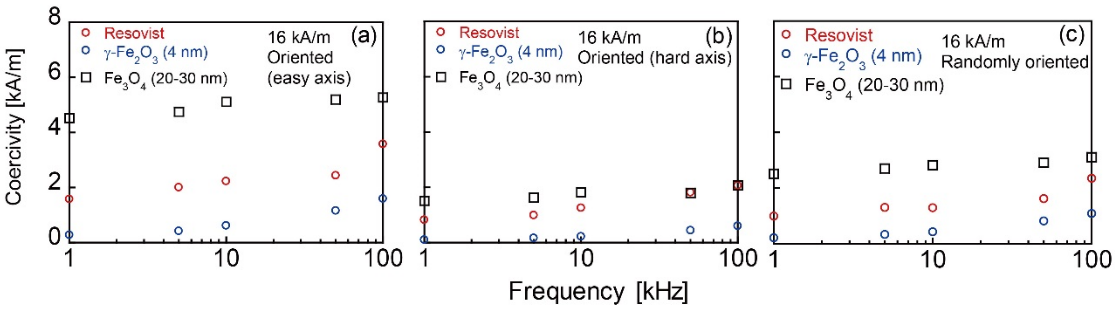

Fig. 8 Frequency characteristics of coercive fields of Resovist, γ-Fe_2O_3, and Fe_3O_4 for (a) easy axis aligned sample, (b) hard axis aligned sample, and (c) randomly oriented sample at a magnetic field of 16 kA/m.

3.3 Specific loss power

The SLP was calculated from the area of the AC hysteresis curve, as shown in Fig. 9. The SLPs of all the samples increased with increase in frequency or amplitude of the magnetic field, which is similar to the result reported in a previous study[21]. Here, the SLP was not linear to the frequency and quantic with the amplitude of the applied field. The SLP in the AC magnetization was given by the superimposition of the hysteresis and magnetic relaxation losses. The effect of the magnetic relaxation shows the non-linear properties to the frequency. The magnetization and coercive field associated with the phase delay of the magnetization to the applied field are decreased and increased with the increase of the frequency[19], respectively. The amplitude and phase delay of the magnetization are represented by the imaginary part of susceptibility χ'', which shows the characteristic response to the frequency. In particular, the χ'' indicates the peak value at the frequency equal to the inverse of the relaxation time τ

shown as $1/2\pi\tau$[16,20,35]. Because the SLP was proportional to the χ''[15], the SLP shows the non-linear response to the frequency. It is also indicated that the SLP normalized by the frequency and amplitude of the applied field was not constant and showed the peak value as the response to the frequency[17].In addition, because the linear response theory of the magnetization to the field amplitude was not applicable in 16 kA/m due to the saturation of the magnetization in the high field amplitude, the SLP was not proportional to quantic with the field amplitude[16]. As shown in Figs. 9(a)–(c), Resovist® has the highest SLP at a field intensity of 4 kA/m. This tendency is consistent with that of the coercive field shown in Fig. 7. As shown in Figs. 9(d)–(f), as the magnetization reversal of the easy axis aligned Fe_3O_4 (20–30 nm) occurs at a field intensity of 16 kA/m, the coercive field is higher. Nevertheless, the SLP is confirmed to be similar to that of Resovist® at high frequencies. Considering the anisotropy constant (K_u) of Fe_3O_4 as 23 kJ/m^3,[15] the calculated peak frequency of Néel relaxation is found to be 0.01 Hz (or lower) using Eq. (2)[11]. Because the rotational degree of the magnetization sufficiently decreased due to longer Néel relaxation time than the cycle of the applied field in the measurement range, the increment of SLP and the coercive field was marginal. The magnetic properties and its relationship with hyperthermia and oriented MNPs have also been studied[36-38]. It is possible that the MNPs form chains even when uniform DC magnetic field is applied. Because the dipole interaction by the chain structure resulted in the effective anisotropy[39,40], the Néel relaxation time in the easy axis of the aligned sample was longer than that in the randomly oriented sample, which also induced the high coercive field and the SLP in the easy axis aligned sample[11].

The ILP denotes the heating capability of particles that is less dependent on the excitation conditions of field intensity and frequency, which can be used to compare the heating property of different samples. At this moment, it was reported that ILP of about 7 nHm^2/kg was obtained at 1 MHz[35]. In this study, ILP of Resovist® with about 4 nHm^2/kg at 100 kHz was obtained with oriented as to be parallel to the exciting magnetic field. Furthermore, the Néel relaxation time of Resovist® was calculated to be in the range of 0.11–36.5 ns using attempt time of 10^{-9} s and anisotropy constant of 4.6 kJ/m^3 in Eq. (1)[15]. From this result, the peak frequency of the Néel relaxation is from 4.3 MHz to 1.3 GHz, which is well above 1 MHz. It can be expected that a further large ILP can be obtained at the excitation frequency of 1 MHz.

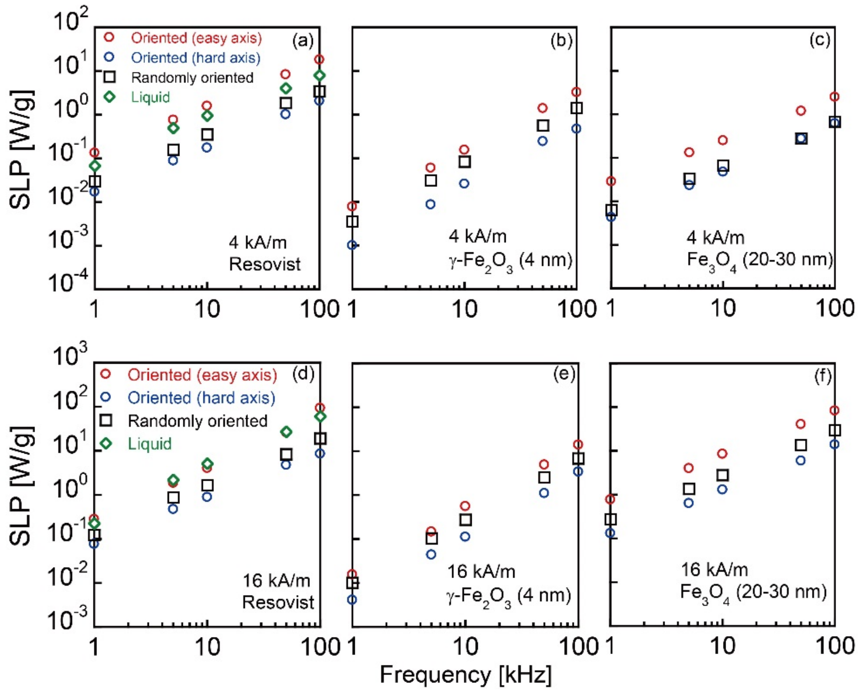

Fig. 9 Frequency characteristics of SLP at field intensities of 4 kA/m and 16 kA/m.

4 Conclusions

In this study, we investigated the magnetization characteristics of Resovist®. Samples oriented along the easy axis were prepared, and the DC and AC magnetization characteristics of the samples aligned in the easy axis and hard axis directions were evaluated, including those of the randomly orientated and liquid samples. The coercive field was found to increase with the increase in the frequency in the easy axis sample, whereas it slightly increased in the hard axis sample even at high frequencies. This shows that the phase delay of the magnetization with respect to the applied magnetic field is considerable in the easy axis sample, and the magnetization sufficiently follows the applied alternating magnetic field even in the high-frequency in the hard axis sample. Moreover, a high-speed Néel relaxation could be experimentally observed. We confirmed that the SLP and ILP, which can be simultaneously obtained from the AC hysteresis curve, can be increased considerably by the easy axis aligned to the direction of the applied field at a field intensity of 16 kA/m and an excitation frequency of 100 kHz. Enhancing the SLP by orientating the particle is potentially realized in clinical application by applying DC field after installing particles to the human body, followed by applying AC field for hyperthermia.

Journal of Magnetism and Magnetic Materials, Volume 473, pp. 148-154, 2019.
DOI: 10.1016/j.jmmm.2018.10.070

References

[1]. A. Jordan, R. Scholz, P. Wust, H. Fähling, R. Felix, Magnetic fluid hyperthermia (MFH): Cancer treatment with AC magnetic field induced excitation of biocompatible superparamagnetic nanoparticles, J. Magn. Magn. Mater. 201 (1999) 413–419.

[2]. B. Gleich, J. Weizenecker, Tomographic imaging using the nonlinear response of magnetic particles, Nature. 435 (2005) 1214–1217.

[3]. M. Arruebo, R. Fernández-Paccheco, M. R. Ibarra, J. Santamaría, Magnetic nanoparticles for drug delivery, Nano Today. 2 (2007) 22–32.

[4]. K. Hayashi, M. Nakamura, W. Sakamoto, T. Yogo, H. Miki, S. Ozaki, M. Abe, T. Matsumoto, K. Ishimura, Superparamagnetic nanoparticle clusters for cancer theranostics combining magnetic resonance imaging and hyperthermia treatment, Theranostics. 3 (2013) 366−376.

[5]. D. Hensley, Z. W. Tay, R. Dhavalikar, B. Zheng, P. Goodwill, C. Rinaldi, S. Conolly, Combining magnetic particle imaging and magnetic fluid hyperthermia in a theranostic platform, Phys. Med. Biol. 62 (2017) 3483−3500.

[6]. I. Sato, M. Umemura, K. Mitsudo, M. Kioi, H. Nakashima, T. Iwai, X. Feng, K. Oda, A. Miyajima, A. Makino, M. Iwai, T. Fujita, U. Yokoyama, S. Okumura, M. Sato, H. Eguchi, I. Tohnai, Y. Ishikawa, Hyperthermia generated with ferucarbotran (Resovist®) in an alternating magnetic field enhances cisplatin-induced apoptosis of cultured human oral cancer cells, J. Physiol. Sci. 64 (2014)177–183.

[7]. R. L. Duschka, H. Wojtczyk, N. Panagiotopoulos, J. Haegele, G. Bringout, T. M. Buzug, J. Barkhausen, F. M. Vogt, Safety measurements for heating of instruments for cardiovascular interventions in magnetic particle imaging (MPI) – first experiences J. Healthc. Eng. 5 (2014) 79–93.

[8]. I. Conde-Leboran, D. Baldomir, C. Martinez-Boubeta, O. Chubykalo-Fesenko, M. del P. Morales, G. Salas, D. Cabrera, J. Camarero, F. J. Teran, D. Serantes, A single picture explains diversity of hyperthermia response of magnetic nanoparticles, J. Phys. Chem. C 119 (2015) 15698−15706.

[9]. S. Dutz and R. Hergt, Magnetic nanoparticle heating and heat transfer on a microscale: Basic principles, realities and physical limitations of hyperthermia for tumour therapy, Int. J. Hyperthermia, 29 (2013) 790–800.

[10]. T. Yoshida, Y. Matsugi, N. Tsujimura, T. Sasayam, K. Enpuku, T. Viereck, M. Schilling, F. Ludwing, Effect of alignment of easy axes on dynamic magnetization of immobilized magnetic nanoparticles, J. Magn. Magn. Mater. 427 (2017) 162–167.

[11]. R. Takeda, S. Ota, T. Yamada, Y. Takemura, Dynamic hysteresis measurement of magnetic nanoparticles with aligned easy axes, J. Magn. Soc. Jpn. 42 (2018) 55–61.

[12]. J. Carrey, B. Mehdaoui, and M. Respaud, Simple models for dynamic hysteresis loop calculations of magnetic single-domain nanoparticles: Application to magnetic hyperthermia optimization, J. Appl. Phys. 109 (2011) 083921.

[13]. L. Néel, Théorie du traînage magnétique des ferromagnétiques en grains fins avec application aux terres cuites, Ann. Geophys. 5 (1949) 99.

[14]. W. F. Brown, Jr., Thermal Fluctuations of a Single-Domain Particle, Phys. Rev. 130 (1963) 1677–1686.

[15]. R. E. Rosensweig, Heating magnetic fluid with alternating magnetic field, J. Magn. Magn. Mater. 252 (2002) 370–374.

[16]. S. Ota, R. Kitaguchi, R. Takeda, T. Yamada, and Y. Takemura, Rotation of Magnetization derived from Brownian relaxation in magnetic fluids of different viscosity evaluated by dynamic hysteresis measurements over a wide frequency range, Nanomater. 6 (2016) 170.

[17]. H. Mamiya, B. Jeyadevan, Hyperthermia effects of dissipative structures of magnetic nanoparticles in large alternating magnetic field, Sci. Rep. 1 (2011) 157.

[18]. T. Yoshida, S. Bai, A. Hirokawa, K. Tanabe, K. Enpuku, Effect of viscosity on harmonic signals from magnetic fluid, J. Magn. Magn. Mater. 380 (2015) 105–110.

[19]. S. Ota, Y. Takemura, Evaluation of easy-axis dynamics in a magnetic fluid by measurement and analysis of the magnetization curve in an alternating magnetic field, Appl. Phys. Express 10 (2017) 085001.

[20]. S. B. Trisnanto, S. Ota, Y. Takemura, Two-step relaxation process of colloidal magnetic nanoclusters under pulsed fields, Appl. Phys. Express 11 (2018) 075001.

[21]. R. D. Corato, A. Espinosa, L. Latrigue, M. Tharaud, S. Chat, T. Pellegrino, C. Ménager, F. Gazeau, C. Wilhelm, Magnetic hyperthermia efficiency in the cellular environment for different nanoparticle designs, Biomaterials 35 (2014) 6400–6411.

[22]. K. M. Krishnan, Biomedical Nanomagnetics: A Spin Through Possibilities in Imaging, Diagnostics, and Therapy, IEEE Trans. Magn. 46 (2010) 2523–2558.

[23]. R. R. Wildeboer, P. Southern, and Q. A. Pankhurst, On the reliable measurement of specific absorption rates and intrinsic loss parameters in magnetic hyperthermia materials, J. Phys. D: Appl. Phys. 47 (2014) 495003.

[24]. H. Kobayashi, A. Hirukawa, A. Tomitaka, T. Yamada, M. jeun, S. Bae, and Y. Takemura, Self-heating property under ac magnetic field and its evaluation by ac/dc hysteresis loops of $NiFe_2O_4$ nanoparticles, J. Appl. Phys. 107 (2010) 09B322.

[25]. M. Coïsson, G. Barrera, F. Celegato, L. Martino, S. N. Kane, S. Raghuvanshi, F. Vinai, P. Tiberto, Hysteresis losses and specific absorption rate measurements in magnetic nanoparticles for hyperthermia applications, Biochim. Biophys. Acta-Gen. Subj. 1861 (2017) 1545–1558.

[26]. S. Ota, T. Yamada, Y. Takemura, Magnetization Reversal and Specific Loss Power of Magnetic Nanoparticles in Cellular Environment Evaluated by AC Hysteresis Measurement, J. Nanomater. 2015 (2015) 9.

[27]. D. Cabrera, A. Coene, J. Leliaert, E. J. Artés-Ibáñez, L. Dupré, N. D. Telling, F. J. Teran, Dynamical magnetic response of iron oxide nanoparticles inside live cells, ACS Nano. 12 (2018) 2741−2752.

[28]. D. Eberbeck, C. L. Dennis, N. F. Huls, K. L. Krycka, C. Grüttner, F. Westphal, Multicore Magnetic Nanoparticles for Magnetic Particle Imaging, IEEE Trans. Magn. 49 (2013) 269–274.

[29]. T. Yoshida, N. B. Othman, K. Enpuku, Characterization of magnetically fractionated magnetic nanoparticles for magnetic particle imaging, J. Appl. Phys. 114 (2013) 173908.

[30]. M. Kallumadil, M. Tada, T. Nakagawa, M. Abe, P. Southern, Q. A. Pankhurst, Suitability of commercial colloids for magnetic hyperthermia, J. Magn. Magn. Mater. 321 (2009) 1509-1513.

[31]. S. Ota, T. Yamada, and Y. Takemura, Dipole-dipole interaction and its concentration dependence of magnetic

Journal of Magnetism and Magnetic Materials, Volume 473, pp. 148-154, 2019.
DOI: 10.1016/j.jmmm.2018.10.070

fluid evaluated by alternating current hysteresis measurement, J. Appl. Phys. 117 (2015) 17D713.

[32]. SA. Shan, DB. Reeves, RM. Ferguson, JB. Weaver, KM. Krishnan, Mixed Brownian alignment and Néel rotations in superparamagnetic iron oxide nanoparticle suspensions driven by an ac field, Phys. Rev. B92 (2015) 094438.

[33]. K. Simeonidis, MP. Morales, M. Marciello, M. Angelakeris, P. Presa, A. LCarrillo, A. Tabero, A. Villanueve, O. CFesenko, D. Serantes, In-situ particles reorientation during magnetic hyperthermia application: Shape matters twice, Sci. Rep. 6 (2016) 38382.

[34]. J. Carrey, N. Hallali, Torque undergone by assemblies of single-domain magnetic nanoparticles submitted to a rotating magnetic field, Phys. Rev. B94 (2016) 184420.

[35]. P. Bender, J. Fock, C. Frandsen, MF. Hansen, C. Balceris, F. Ludwig, O. Posth, E. Wetterskog, Lk. Bogart, P. Southern, W. Szczerba, L. Zeng, K. Witte, C. Grüttner, F. Westphal, D. Honecker, D. G-Alonso, L. F. Barquín, C. Johansson, Relating Magnetic Properties and High Hyperthermia Performance of Iron Oxide Nanoflowers, J. Phys. Chem. C122 (2018) 3068–3077.

[36]. I. Conde-Leborán, D. Serantes, D. Baldomir, Orientation of the magnetization easy axes of interacting nanoparticles: Influence on the hyperthermia properties, J. Magn. Magn. Mater. 380 (2015) 321–324.

[37]. I. Andreu, E. Natividad, L. Solozábal, and O. Roubeau, Nano-objects for Addressing the Control of Nanoparticle Arrangement and Performance in Magnetic Hyperthermia, ACS Nano. 9 (2015) 1408–1419.

[38]. P. de la Presa, Y. Luengo, V. Velasco, M. P. Morales, M. Iglesias, S. Veintemillas-Verdaguer, P. Crespo, and A. Hernando, Particle Interactions in Liquid Magnetic Colloids by Zero Field Cooled Measurements: Effects on Heating Efficiency, J. Phys. Chem. C119 (2015) 11022–11030.

[39]. L. C. Branquinho, M. S. Carrião, A. S. Costa, N. Zufelato, M. H. Sousa, R. Miotto, R. Ivkov and A. F. Bakuzis, Effect of magnetic dipolar interactions on nanoparticle heating efficiency: Implications for cancer hyperthermia, Sci. Rep. 3 (2013) 2887.

[40]. C. Martinez-Boubeta, K. Simeonidis, A. Makridis, M. Angelakeris, O. Iglesias, P. Guardia, A. Cabot, L. Yedra, S. Estradé, F. Peiró, Z. Saghi, P. A. Midgley, I. Conde-Leborán, D. Serantes and D. Baldomir, Learning from Nature to Improve the Heat Generation of Iron-Oxide Nanoparticles for Magnetic Hyperthermia Applications, Sci. Rep. 3 (2013) 1652.

Journal of Magnetism and Magnetic Materials, Volume 473, pp. 148-154, 2019.
DOI: 10.1016/j.jmmm.2018.10.070

Supplementary material

S1-DC magnetization curves at field intensity of 4 kA/m

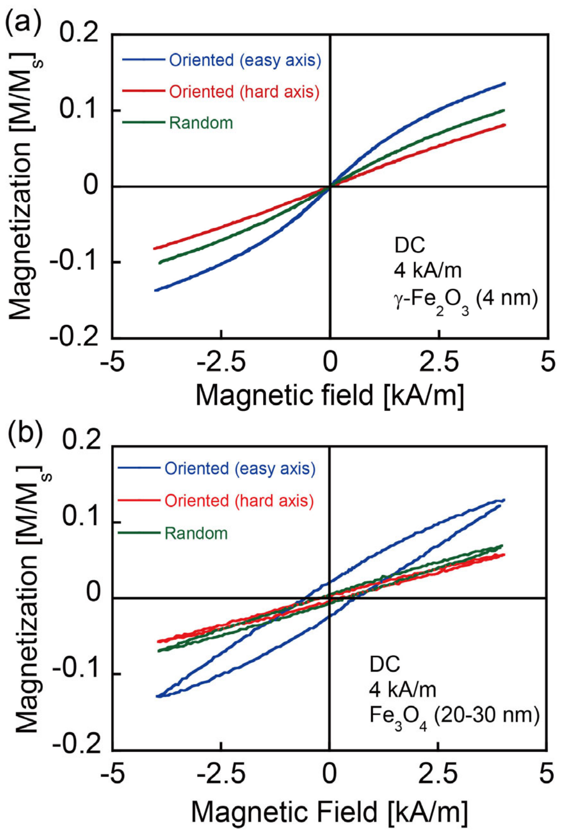

Fig. S1 DC magnetization curves of (a) γ-Fe_2O_3 (4 nm) and (b) Fe_3O_4 (20–30 nm) at field intensity of 4 kA/m.

Journal of Magnetism and Magnetic Materials, Volume 473, pp. 148-154, 2019.
DOI: 10.1016/j.jmmm.2018.10.070

S2- DC and AC magnetization curves of γ-Fe_2O_3 (4 nm)

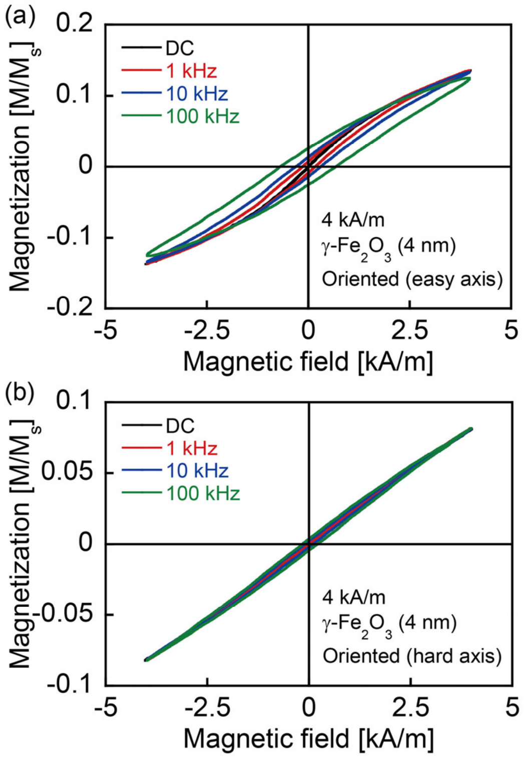

Fig. S2 DC and AC magnetization curves of γ-Fe_2O_3 (4 nm) nanoparticles at field intensity of 4 kA/m. Direction of applied field was along (a) easy axis and (b) hard axis.